# Fusing spectral and textural information in near-infrared hyperspectral imaging to improve green tea classification modelling

Puneet Mishra[1*], Alison Nordon[1*], Mohd Shahrimie Mohd Asaari[2], Guoping Lian[3,4], Sally Redfern[3]

[1]*WestCHEM, Department of Pure and Applied Chemistry and Centre for Process Analytics and Control Technology, University of Strathclyde, Glasgow, G1 1XL, United Kingdom*

[2]*Vision Lab, Department of Physics, Campus Drie Eiken, University of Antwerp, Edegemsesteenweg 200-240, 2610, Antwerp, Belgium*

[3]*Unilever R&D Colworth, Colworth Science Park, Sharnbrook, Bedford, MK44 1LQ, United Kingdom*

[4] *Department of Chemical and Process Engineering, University of Surrey, Guildford GU2 7XH, United Kingdom*

*Corresponding authors email: puneet.mishra@strath.ac.uk , alison.nordon@strath.ac.uk*

## Abstract

Hyperspectral imaging (HSI) can acquire data in two modes: imaging and spectroscopy, revealing the spatially-resolved spectral properties of materials. Traditional HSI processing in the close-range domain primarily focuses on the spectral information with minimal utilisation of the spatial information present in the data. The present work describes a methodology for utilising the spatial information present in HSI data to improve classification modelling over that achievable with spectral information alone. The methodology has been evaluated using near infrared (NIR) HSI data of sixteen green tea products from seven different countries.

The methodology involves selecting and sharpening an image plane to enhance the textural details. The textural information is then extracted from the statistical properties of the grey level co-occurrence matrix (GLCM) of the sharpened image plane using a moving window operation. Finally, the textural properties are combined with the spectral information using one of the three different levels of data fusion, i.e. raw data level, feature level and decision level. Raw data-level fusion involved concatenating the spectral and textural data before performing the classification task. The feature-level fusion involved performing principal component analysis (PCA) on spectral and textural information and combining the PC scores obtained prior to performing classification. Decision-level fusion involved a majority voting scheme to enhance the final classification maps. All the classification tasks were performed using multi-class support vector machine (SVM) models. The results showed that combining the textural and spectral information during modelling resulted in improved classification of the sixteen green tea products compared to models built using spectral or textural information alone.

*Keywords:* chemical imaging; texture; support vector machine (SVM); grey level co-occurrence matrix (GLCM); data fusion; green tea.

# 1. Introduction

Computer vision and image processing have benefited from the exploration of spatially-resolved physical properties of materials in analytical chemistry [1]. The combination of imaging with spectroscopy, known as hyperspectral imaging (HSI), has complemented imaging by allowing simultaneous exploration of spatial and spectral properties of materials in a fast and non-destructive way. Although HSI was primarily developed for remote sensing [2], it is now a well-established technique in close-range laboratory settings [3, 4, 5, 6]. HSI

has been used for the study of a wide range of food products such as wheat flour [7], olive oil [8], herbal tea [9], seeds [10], coffee [11], beans [12] and many more [13].

The information generated by HSI takes the form of hypercubes where the first two dimensions represent the spatial information of the imaged scene and the third dimension adds the spectral information to the pixels [12]. The extraction of meaningful information from the hypercube requires advanced pattern recognition and data modelling. Although, HSI data is rich in information, not all the information present is needed to perform the data modelling. The traditional HSI processing approach includes selection of the region of interest (ROI) over the image plane to extract the relevant spectra. The selected spectra are then used to perform different types of modelling such as data visualisation, regression, and classification. The models developed are used to predict the scores for each pixel to represent prediction or classification maps [14]. This modelling approach aids in visualising the spatial distribution of the predicted values or classes. However, the complementary information present in the spatial domain, e.g., texture, is not generally used in the construction of calibration models based on spectra [15]. In the predecessor of close-range HSI, i.e. remote sensing, the importance of information present in the spatial domain of HSI is well realised. In particular, utilising the spatial information to improve classification modelling is widely employed [16]. The spatial information can be used either pre or post-classification modelling to improve the classification accuracies and classification maps.

There are some extra benefits to the application of HSI in close-range settings, compared to the remote-sensing domain, which further motivates the use of spatial information. One of the benefits is the high spatial resolution of the images, which reduces the number of mixed pixels in the imaged scene leading to improved image quality. The other is the artificial dark-field illumination used to enhance the contrast of regions where illumination interferes with the edges, scratches, imprints, slots and elevations over the imaging scene, leading to detailed

information about the physical features of samples [17]. The spatial information that is primarily of interest in the case of close-range HSI is textural. Texture can be understood as a quantitative measure of the arrangement of intensities in a region [18]. Therefore, it is necessary to calculate texture from statistical analysis of an image plane. There are different ways of extracting textural information from an image plane. Estimating the grey level co-occurrence matrices (GLCMs) has gained widespread interest in the close-range HSI processing domain [19, 20, 21, 22, 23, 24, 25]. A reason for its popularity is that the statistical properties extracted from GLCMs can be used to represent, compare and classify texture. Since the GLCM-based texture calculation can only be performed on a monochromatic image, an image at a single wavelength is usually selected from the HS image and subjected to GLCM analysis [20, 24]. Furthermore, utilising textural information in conjunction with spectral information can be realised in a data fusion approach to combine the two types of information at three different levels, i.e., low, middle and high. The low-level data fusion of spectral and textural information utilises the spectral and textural data in raw form and performs concatenation of the data matrices before the data modelling. Mid-level fusion involves doing some feature transformation prior to performing the fusion such as utilising principal component analysis (PCA) to capture the most important variation in the feature vector and later concatenating the scores obtained for the corresponding features. High-level involves decision-level fusion where the output from different models is usually fused based on some decision criteria to enhance the final output such as classification maps.

The aim of this work is to present a methodology for fusing spectral and textural information to improve the modelling of near-infrared (NIR) HSI data. To demonstrate the potential of fusing textural and spectral information, the classification of sixteen green tea products from seven different countries was considered. High-quality green tea products are mainly characterised by the flavour that they impart, which involves two primary sensory

perceptions, i.e. taste and aroma. The distinct taste and aroma of any tea product are derived from its geographical origin as they are unique to the climate and soil conditions in which the plants were grown. Typically, discrimination of green tea products via sensory analysis is performed using an expert human panel. Sensory analysis involves assessment of tea products in leaf and/or extracted liquor form on the basis of appearance, colour, aroma and taste, along with the overall quality of the samples. However, distinguishing tea products based on sensory analysis is a time-consuming and expensive task as it requires an expert human panel. Furthermore, sensory analysis is subjective, and it can be inconsistent and unpredictable owing to physiological and psychological differences between tasters [26]. One more limitation is that the expert panel cannot be used as an on-line technique for grading of tea products [27]. In recent years, different analytical techniques have been explored for assessment of tea products of which HSI is one. NIR HSI, in comparison to visible HSI, provides access to the chemical information present in samples. NIR HSI has recently been used to discriminate between different types of tea products [28], although only the spectral information was used to build the classification models. However, leaf tea products also have a rich amount of textural detail present in their leaves; such textural information has previously been used to classify tea products [17, 29]. However, utilising texture alone is not a robust modelling solution as textural properties are affected by variations in illumination intensity [30]. Therefore, in this work, we utilise the textural information as supplementary information to enhance NIR spectroscopy-based classification of green tea products.

# 2. Material and methods

## 2.1. Samples

Sixteen green tea samples, differing in geographical origin, were sourced in loose-leaf form from Unilever R&D, Colworth Science Park, United Kingdom. All the samples were provided in sealed packaging and were stored at ambient temperature until analysis. All

samples were green in colour and exhibited some textural differences owing to variations in the shape and size of the leaves. The sixteen samples originated from seven different countries: Argentina (one), South India (five), Sri Lanka (two), China (two), Japan (two), Kenya (three) and Sumatra (one). Imaging experiments were performed by presenting the sample in a circular black plastic cap (diameter = 3.3 cm, depth = 1.3 cm). The sixteen tea samples were each analysed in a different cap to avoid any cross-contamination.

## 2.2. Hyperspectral imaging measurements

Imaging was performed with a push-broom line scan NIR HSI camera (*Model name*: RED EYE 1.7) from INNO-SPEC (Nurnberg, Germany). The camera has an InGaAs sensor and generates a spatial map of 320 x 256 pixels, and has pixel dimensions of 30 x 30 $\mu m^2$. Images were acquired over the spectral range of 950 – 1765 nm with a spectral resolution of 3.2 nm. Two halogen light sources, each with a power of 50 W, were used to illuminate the samples. For image acquisition, the sixteen tea samples were placed on the translation stage, which was controlled via an independent stage motor system (Zolix TSA 200 BF). The speed of the translation stage, 2.5 mm $s^{-1}$, was optimised using a checkerboard to avoid any distortion in the shape of the image arising from the overlapping of spectral and spatial information. The distance from the lens to the translation stage was 15 cm. Prior to acquisition of an image, a set of white (Spectralon diffuse reflectance standard) and dark references were recorded for radiometric calibration. Each image comprised more than 2000 pixels (spectra) per individual green tea sample and was acquired using an integration time of 300 ms.

## 2.3. Data analysis

### 2.3.1. Image pre-processing

Variations in signal arising from illumination intensity, the detector sensitivity and the transmission properties of the optics were corrected by radiometric calibration utilising dark and white reference images. The correction was performed for every pixel in the HS image according to equation (1):

$$I_{R(i,j,k)} = \frac{I_{raw(i,j,k)} - I_{dark(i,j,k)}}{I_{white(i,j,k)} - I_{dark(i,j,k)}} \quad (1)$$

where, $I_R$ is the calibrated reflectance, $I_{raw}$ is the raw intensity measured from the test sample, $I_{dark}$ is the intensity of the dark response, $I_{white}$ is the intensity of the uniform white reference, and *i* and *j* are spatial coordinates and *k* is the wavelength of the image. The spectral range of the hypercube was reduced from 950 – 1765 nm to 967.11 – 1700 nm to remove noise. A moving window Savitzky-Golay (SAVGOL) filter [31] (15-point width and second order polynomial) was applied to each pixel of the image to remove random noise, e.g. spikes, from spectra. Further, to reduce light scattering effects arising from inhomogeneity of the sample surface, the spectra were normalised using the standard normal variate (SNV) [32]. Smoothing and normalisation were performed using the *savgol* and *snv* functions, respectively, from PLS_Toolbox (version 8.11, Eigenvector Research Inc., USA).

### 2.3.2. Texture estimation

#### *2.3.2.1. Selection of image plane*

Textural analysis requires a single image plane to enable extraction of the GLCM properties. Since some spectral bands are noisy compared to others in HSI, the best image plane can be chosen on the basis of two different image quality parameters: the peak signal-to-noise ratio (PSNR) and the structural similarity index measure (SSIM). The PSNR and SSIM were calculated with respect to the mean image plane (reference image), obtained from averaging the intensities of pixels along the spectral dimension. The PSNR can be calculated using equation (2):

$$PSNR = 10\ log_{10}\left(\frac{peakval^2}{MSE}\right) \quad (2)$$

where *peakval* is either specified by the user or selected from a range that is dependent on the image datatype (e.g. 255 for a uint8 image) and *MSE* is the mean square error between the chosen image plane and the reference image.

The SSIM [33] is based on the computation of three terms, namely the luminance term (*l*), the contrast term (*c*) and the structural term (*s*). The overall index is a multiplicative combination of the three terms calculated by equation (3):

$$SSIM(x,y) = [l(x,y)]^{\alpha}.[c(x,y)]^{\beta}.[s(x,y)]^{\gamma} \qquad (3)$$

where

$$l(x,y) = \frac{2\mu_x\mu_y + C_1}{\mu_x^2 + \mu_y^2 + C_2}$$

$$c(x,y) = \frac{2\sigma_x\sigma_y + C_2}{\sigma_x^2 + \sigma_y^2 + C_2}$$

$$s(x,y) = \frac{\sigma_{xy} + C_3}{\sigma_x\sigma_y + C_3}$$

and $\mu_x$ and $\mu_y$ are the local means, and $\sigma_x$ and $\sigma_y$ are the standard deviations of images *x* (reference image) and *y* (chosen image plane), respectively, $\sigma_{xy}$ is the cross-covariance for images *x* and *y*, $\alpha, \beta$ and $\gamma$ are exponent terms, which were set to 1, and $C_1 = (k_1L)^2$, $C_2 = (k_2L)^2$ and $C_3 = C_2/2$ where $k_1 = 0.01$, $k_2 = 0.03$ and $L = 255$. The best image plane was selected based on the maximum PSNR and SSIM.

#### 2.3.2.2. Sharpening of the image plane

The raw HS images obtained had soft edges owing to the limited focus and/or low spatial resolution of the camera resulting in low contrast between adjacent pixel intensities. Therefore, the image plane was sharpened to enhance the textural details. The enhanced textural details obtained with sharpening should result in more accurate calculation of the GLCM properties. Typically, the aim of sharpening is to increase the contrast along the edges where different colours meet. In the present work, the unsharp masking technique was used to perform image sharpening. This technique sharpens the image by first estimating a "blurred" negative image mask from the original image, which is then subtracted from the original image creating an image that is less blurry than the original [34]. Textural analysis

was then performed on the sharpened image via estimation of the statistical properties of the GLCM.

#### 2.3.2.3. Estimating GLCM properties

*Figure 1: Schematic of the window operation performed for extracting textural features.*

The textural information of the image has variations in the greyscale as a function of spatial position. Different pixels in the image share spatial relationships in terms of greyscale intensities, which is spatial correlation. A common method to represent the relationship between greyscale pixels is via GLCMs [19, 20, 21, 22, 23, 24, 25]. The GLCM aims to describe the textural information present in the image by defining how often pairs of pixels with a specific value and spatial relationship occur in an image. The GLCM is a square matrix whose elements represent the probabilities of a pixel being at a distance from another pixel with a fixed spatial relationship. These values of the elements represent the conditional probabilities of all pairwise combinations of greyscale levels in the spatial window. Statistical measures can further be applied to these conditional probabilities to generate the textural properties. In the present work, twenty different statistical measures were estimated resulting in twenty different textural information maps. The twenty statistical properties considered were the correlation, autocorrelation, contrast, cluster prominence, cluster shade, dissimilarity, energy, entropy, homogeneity, variance, sum average, sum variance, sum entropy, difference variance, difference entropy, two information measures of correlation, inverse moment difference, inverse difference normalised and inverse difference moment normalised. Further information on the use of statistical metrics for estimating textural properties can be found in [35, 36, 37]. In the present work, the GLCM estimation was performed utilising the “graycomatrix” command in Matlab (R2016b, Mathworks, USA). A square window with a size of 11 x 11 pixels$^2$, which was moved over the image plane (see

Figure 1), was used for the GLCM estimation. The window size was selected based on the number of pixels required to cover the largest tea leaves, and was an odd number to give equal coverage of the pixels around the centre pixel. In this process, the greyscale intensity of the centre pixel was replaced with the estimated textural property of the GLCM. To make the GLCM uniform around the exterior area of the sample, a patch mask was defined, which included replacing the individual pixel intensity values by their mean intensities. Textural analysis resulted in the calculation of 20 image planes corresponding to the 20 statistical metrics given above; all 20 textural image planes were used in subsequent analysis.

### 2.3.3. Feature transformation with PCA

In the present work, two PCA models were built to transform the spectral and textural information separately. The number of principal components was selected such that >99% of the variance in the data was retained. The PCA decomposition was performed in Matlab utilising the PLS_Toolbox.

### 2.3.4. Data fusion scheme

*Figure 2: Schematic for raw data-level and feature-level fusion.*

Once the 20 textural features were obtained from the data, the fusion of textural information with the spectral information was performed. The scheme for raw data-level and feature-level fusion is depicted in Figure 2. Raw data-level fusion was performed by concatenating the texture with the spectral information. In the case of feature-level fusion, two separate PCA models were constructed to extract the relevant features from the spectral and textural cubes. The extracted features were then concatenated before performing the classification modelling. In the case of decision-level fusion, all the classification maps obtained from raw- and feature-level data fusion were used within a majority voting scheme and the final

classification map was updated.

### *2.3.5. Classification with support vector machines*

In the chemometrics domain, there are different methods to perform the classification of spectral features [38]. However, in the image processing domain the support vector machine (SVM) has gained popularity for the classification of fused spectral and textural information [39]. Classification of the 16 green tea products was performed using multi-class error correcting output code (ECOC) models containing SVM binary learners, using a one-versus-one coding design. High dimensional mapping of the data was performed using a quadratic kernel. For every green tea sample, spectra and/or textural information were extracted from 400 pixels, selected at random from the image, leading to 6400 pixels in total for the calibration of the classification models. The models were cross-validated with the 10-fold cross-validation method. This whole calibration procedure was performed with 100 iterations with the mean validation accuracy and standard deviation recorded. The trained classifiers were later used to generate the classification maps for the tea samples contained in the image, which comprised more than 2000 pixels per sample. The ECOC-SVM models were implemented in Matlab using the Statistics and Machine Learning Toolbox (R2016b).

## 3. Results

*Figure 3: Criteria used for selection of the best image plane on which to perform sharpening and textural analysis: a) SSIM and b) PSNR for all image planes in the range 967.11 – 1700 nm.*

Figure 3 presents the SSIM and PSNR obtained for each HSI image plane in the range 967.11 – 1700 nm. It can be seen in Figure 3(a), that the SSIM value was highest for the image plane at 1381 nm. The higher the SSIM value, the more similar the image of interest is to the

reference image. For example, an SSIM value of one signifies that the image is exactly the same as the reference image, whereas, a SSIM value of zero indicates that there is no similarity between the image plane and the reference image. In Figure 3(b), it can be seen that the image plane at 1381 nm also has the highest PSNR value. A high PSNR value indicates that there is more information present (relative to the noise) in the image plane at 1381 nm compared to image planes at other wavelengths. The image plane corresponding to 1381 nm is presented in Figure 4(a). Figure 4(b) presents the same image plane after sharpening. It can be seen that before sharpening, the image plane is blurred, however, this is reduced after sharpening and the textural details are more evident.

*Figure 4: Greyscale images produced using the image plane at 1381 nm (a) without and (b) with sharpening.*

*Figure 5: Mean classification accuracies (in percent) of the 16 green tea products obtained for the calibration samples (pixels) using models built with raw data and PCA features. In both cases, models were built using spectral information alone, textural information alone and fused spectral and textural information. The error bars denote ±1 standard deviation (n = 100).*

Figure 5 presents the mean classification accuracies of the 16 green tea products obtained for the calibration samples (pixels) using multi-class SVM models developed with spectral and textural information. The accuracies are presented as the mean ± one standard deviation for 100 iterations. Confusion matrices showing classification accuracies for individual classes obtained using raw data and feature-level SVM models are given in Figures S1 and S2, respectively, of the Supplementary Material. It can be seen from Figure 5 that the models built with the spectral information alone were more accurate than those constructed using only textural information. Combining textural information with spectral information resulted in an improvement in the model accuracy. Improvements were observed for both raw data-level fusion as well as feature-level fusion. The model accuracy for fusion of data at the raw

level was higher compared than that at the feature level. It could be that the features extracted using PCA contain less information than the raw data. The features were selected so as to retain 99% of the variance in the data whereas the raw data retains all of the information. and therefore, this could account for the higher accuracy of the raw data models. Use of supervised feature selection algorithms such as partial least squares discriminant analysis (PLS-DA) could improve the performance of the feature-level models.

*Figure 6: Classification maps for the 16 green tea products obtained from SVM modelling of (a). raw spectral information, (b). raw textural information, and (c). concatenated raw spectral and textural information.*

*Figure 7: Classification maps for the 16 green tea products obtained from SVM modelling of (a). PCA features extracted from spectral information, (b). PCA features extracted from textural information, and (c). concatenated PCA features from spectral and textural information.*

*Figure 8: Classification maps for the 16 green tea products obtained from decision-level data fusion, using a majority voting scheme, of the six classification maps obtained from SVM modelling of spectral information, textural information, and spectral and textural information using raw data (Figure 6) and PCA features (Figure 7).*

Figure 6 and Figure 7 presents the classification maps for the 16 green tea products obtained from application of the raw data and feature-level SVM models, respectively, to the complete image. Every circular object in the classification maps is a different green tea sample, comprising more than 2000 pixels per sample, and the different colours reflect different classes. In Figure 6, the three classification maps were obtained from three different SVM models built using raw spectral data (Figure 6a), raw textural data (Figure 6b) and concatenated raw spectral and textural data (Figure 6c). Similarly, in Figure 7 the three classification maps were obtained from three different SVM models built using the scores obtained from PCA of spectral data (Figure 7a), the scores obtained from PCA of textural data (Figure 7b) and the concatenated scores obtained from separate PCA models of spectral and textural data (Figure 7c). Figure 8 provides the output of a majority voting scheme performed on all six classification maps, i.e., three from the raw data (Figure 6) and three

from the extracted features (Figure 7). Majority voting was performed by assigning the pixel value to the class that occurred most frequently in all six classification maps. It can be seen from visual inspection of Figures 6, 7 and 8 that improved classification maps (i.e. an increase in the number of pixels inside the circular area belonging to the same class) were obtained for models built using fused spectral and textural information. This improvement can be quantified by calculating the percentage of correctly classified pixels as shown in Figure 9. It can be seen that the highest values were obtained for models built using raw data-level fusion (~84%), followed by decision-level fusion (~83%), with the least number of correctly classified pixels obtained using feature-level data fusion (~78%). Fusion of spectral and textural information at all levels (raw, feature and decision) gave improved model accuracies compared to spectral or textural information alone at the relevant level (i.e. raw or PCA features) leading to an improvement in the classification maps. These results are consistent with HSI studies of meat products [20, 21, 23, 24, 25] where improved classification or property prediction was obtained with models built using both spectral and textural information.

*Figure 9: Percentage of pixels correctly identified in the classification maps for the 16 green tea products obtained using six different SVM models and decision-level fusion by majority voting.*

# 4. Conclusions

The spectral and spatial domains of HSI generate complementary information, and synergistic processing of the information can lead to enhanced classification model accuracies and improved classification maps. The present work fused spectral and textural data at three different levels to demonstrate the usefulness of textural information in HSI for classification of green teas. The highest classification accuracy (97.30 ± 0.12% for the

calibration samples) was obtained using the raw data-level fusion, which was superior to that obtained for feature-level data fusion. In this case, feature extraction resulted in information loss. However, use of supervised feature selection methods, such as PLS-DA, could improve the performance of the feature-level models. Decision-level fusion provided classification maps of comparable quality to those obtained using raw data-level fusion. In conclusion, the extracted textural information is always complementary as it can support the development of enhanced understanding of the samples and further model improvement. However, it should be noted that the decision to use the textural information in data modelling has to be based on the samples imaged, as samples with high textural information can contribute positively to model improvement whereas model with no such textural details will merely increase the computation load. Therefore, the methodology developed will be useful in the assessment of a variety of food products (e.g., tea, spices, meat and fruit) where consideration of both spectral and textural information is required for, e.g., quality control and counterfeit detection.

## Acknowledgment

This work has received funding from the European Union's Horizon 2020 research and innovation programme named 'MODLIFE' (Advancing Modelling for Process-Product Innovation, Optimization, Monitoring and Control in Life Science Industries) under the Marie Sklodowska-Curie grant agreement number 675251.

The authors also acknowledge the Centre for Hyperspectral Imaging at the University of Strathclyde, particularly Julius Tschannerl and Prof. Stephen Marshall for their kind help in performing the HSI experiments.

## References

1. L.F. Capitán-Vallvey, N. López-Ruiz, A. Martínez-Olmos, M.M. Erenas, A.J. Palma, Recent developments in computer vision-based analytical chemistry: A tutorial review, Anal. Chim. Acta. 899 (2015) 23–56. doi:https://doi.org/10.1016/j.aca.2015.10.009.
2. A.F. Goetz, G. Vane, J.E. Solomon, B.N. Rock, Imaging spectrometry for Earth remote sensing., Science. 228 (1985) 1147–1153. doi:10.1126/science.228.4704.1147.
3. A.A. Gowen, C.P. O'Donnell, P.J. Cullen, G. Downey, J.M. Frias, Hyperspectral imaging – an emerging process analytical tool for food quality and safety control, Trends Food Sci. Technol. 18 (2007) 590–598. doi:https://doi.org/10.1016/j.tifs.2007.06.001.
4. G. Elmasry, M. Kamruzzaman, D.-W. Sun, P. Allen, Principles and Applications of Hyperspectral Imaging in Quality Evaluation of Agro-Food Products: A Review, Crit. Rev. Food Sci. Nutr. 52 (2012) 999–1023. doi:10.1080/10408398.2010.543495.
5. Y.-Z. Feng, D.-W. Sun, Application of Hyperspectral Imaging in Food Safety Inspection and Control: A Review, Crit. Rev. Food Sci. Nutr. 52 (2012) 1039–1058. doi:10.1080/10408398.2011.651542.
6. M. Manley, Near-infrared spectroscopy and hyperspectral imaging: non-destructive analysis of biological materials, Chem. Soc. Rev. 43 (2014) 8200–8214. doi:10.1039/C4CS00062E.
7. P. Mishra, C.B.Y. Cordella, D.N. Rutledge, P. Barreiro, J.M. Roger, B. Diezma, Application of independent components analysis with the JADE algorithm and NIR hyperspectral imaging for revealing food adulteration, J. Food Eng. 168 (2016) 7–15.
8. D.M. Martínez Gila, P. Cano Marchal, J. Gámez García, J. Gómez Ortega, On-line system based on hyperspectral information to estimate acidity, moisture and peroxides

in olive oil samples, Comput. Electron. Agric. 116 (2015) 1–7. doi:https://doi.org/10.1016/j.compag.2015.06.002.

9. M. Sandasi, W. Chen, I. Vermaak, A. Viljoen, Non-destructive quality assessment of herbal tea blends using hyperspectral imaging, Phytochem. Lett. 24 (2018) 94–101. doi:https://doi.org/10.1016/j.phytol.2018.01.016.
10. C. Nansen, G. Zhao, N. Dakin, C. Zhao, S.R. Turner, Using hyperspectral imaging to determine germination of native Australian plant seeds, J. Photochem. Photobiol. B Biol. 145 (2015) 19–24. doi:https://doi.org/10.1016/j.jphotobiol.2015.02.015.
11. N. Caporaso, M.B. Whitworth, M.S. Fowler, I.D. Fisk, Hyperspectral imaging for non-destructive prediction of fermentation index, polyphenol content and antioxidant activity in single cocoa beans, Food Chem. 258 (2018) 343–351. doi:https://doi.org/10.1016/j.foodchem.2018.03.039.
12. K. Phuangsombut, T. Ma, T. Inagaki, S. Tsuchikawa, A. Terdwongworakul, Near-infrared hyperspectral imaging for classification of mung bean seeds, Int. J. Food Prop. 21 (2018) 799–807. doi:10.1080/10942912.2018.1476378.
13. Y. Liu, H. Pu, D.-W. Sun, Hyperspectral imaging technique for evaluating food quality and safety during various processes: A review of recent applications, Trends Food Sci. Technol. 69 (2017) 25–35. doi:https://doi.org/10.1016/j.tifs.2017.08.013.
14. J.M. Amigo, H. Babamoradi, S. Elcoroaristizabal, Hyperspectral image analysis. A tutorial, Anal. Chim. Acta. 896 (2015) 34–51. doi:https://doi.org/10.1016/j.aca.2015.09.030.
15. A. de Juan, Hyperspectral image analysis. When space meets Chemistry, J. Chemom. 32 (2018) e2985–n/a. doi:10.1002/cem.2985.

16. L. Wang, C. Shi, C. Diao, W. Ji, D. Yin, A survey of methods incorporating spatial information in image classification and spectral unmixing, Int. J. Remote Sens. 37 (2016) 3870–3910. doi:10.1080/01431161.2016.1204032.
17. A. Laddi, S. Sharma, A. Kumar, P. Kapur, Classification of tea grains based upon image texture feature analysis under different illumination conditions, J. Food Eng. 115 (2013) 226–231. doi:https://doi.org/10.1016/j.jfoodeng.2012.10.018.
18. M. Tuceryan, A.K. Jain, Texture analysis, in: Handb. Pattern Recognit. Comput. Vis., World Scientific, 1993: pp. 235–276.
19. J. Ma, D.-W. Sun, J.-H. Qu, H. Pu, Prediction of textural changes in grass carp fillets as affected by vacuum freeze drying using hyperspectral imaging based on integrated group wavelengths, LWT - Food Sci. Technol. 82 (2017) 377–385. doi:https://doi.org/10.1016/j.lwt.2017.04.040.
20. C. Garrido-Novell, A. Garrido-Varo, D. Pérez-Marín, J.E. Guerrero, Using spectral and textural data extracted from hyperspectral near infrared spectroscopy imaging to discriminate between processed pork, poultry and fish proteins, Chemom. Intell. Lab. Syst. 172 (2018) 90–99. doi:https://doi.org/10.1016/j.chemolab.2017.11.011.
21. D. Yang, D. He, A. Lu, D. Ren, J. Wang, Combination of spectral and textural information of hyperspectral imaging for the prediction of the moisture content and storage time of cooked beef, Infrared Phys. Technol. 83 (2017) 206–216. doi:https://doi.org/10.1016/j.infrared.2017.05.005.
22. S. Fan, B. Zhang, J. Li, C. Liu, W. Huang, X. Tian, Prediction of soluble solids content of apple using the combination of spectra and textural features of hyperspectral reflectance imaging data, Postharvest Biol. Technol. 121 (2016) 51–61. doi:https://doi.org/10.1016/j.postharvbio.2016.07.007.

455 23. D. Liu, H. Pu, D.-W. Sun, L. Wang, X.-A. Zeng, Combination of spectra and texture
456 data of hyperspectral imaging for prediction of pH in salted meat, Food Chem. 160
457 (2014) 330–337. doi:https://doi.org/10.1016/j.foodchem.2014.03.096.
458 24. H. Pu, D.-W. Sun, J. Ma, J.-H. Cheng, Classification of fresh and frozen-thawed pork
459 muscles using visible and near infrared hyperspectral imaging and textural analysis,
460 Meat Sci. 99 (2015) 81–88. doi:https://doi.org/10.1016/j.meatsci.2014.09.001.
461 25. W. Cheng, D.-W. Sun, H. Pu, Y. Liu, Integration of spectral and textural data for
462 enhancing hyperspectral prediction of K value in pork meat, LWT - Food Sci.
463 Technol. 72 (2016) 322–329. doi:https://doi.org/10.1016/j.lwt.2016.05.003.
464 26. D. Huo, Y. Wu, M. Yang, H. Fa, X. Luo, C. Hou, Discrimination of Chinese green tea
465 according to varieties and grade levels using artificial nose and tongue based on
466 colorimetric sensor arrays, Food Chem. 145 (2014) 639–645.
467 doi:https://doi.org/10.1016/j.foodchem.2013.07.142.
468 27. W. He, X. Hu, L. Zhao, X. Liao, Y. Zhang, M. Zhang, J. Wu, Evaluation of Chinese
469 tea by the electronic tongue: Correlation with sensory properties and classification
470 according to geographical origin and grade level, Food Res. Int. 42 (2009) 1462–
471 1467. doi:https://doi.org/10.1016/j.foodres.2009.08.008.
472 28. P. Mishra, A. Nordon, J. Tschannerl, G. Lian, S. Redfern, S. Marshall, Near-infrared
473 hyperspectral imaging for non-destructive classification of commercial tea products,
474 J. Food Eng. 238 (2018) 70-77. doi:https://doi.org/10.1016/j.jfoodeng.2018.06.015.
475 29. Z. Tang, Y. Su, M.J. Er, F. Qi, L. Zhang, J. Zhou, A local binary pattern based texture
476 descriptors for classification of tea leaves, Neurocomputing. 168 (2015) 1011–1023.
477 doi:https://doi.org/10.1016/j.neucom.2015.05.024.
478 30. N.R. Sarkar, Machine vision for quality control in the food industry, Instrum.
479 Methods Qual. Assur. Foods. (1991) 167–187.

480 31. A. Savitzky, M.J.E. Golay, Smoothing and Differentiation of Data by Simplified
481 Least Squares Procedures., Anal. Chem. 36 (1964) 1627–1639.
482 doi:10.1021/ac60214a047.
483 32. R.J. Barnes, M.S. Dhanoa, S.J. Lister, Standard Normal Variate Transformation and
484 De-Trending of Near-Infrared Diffuse Reflectance Spectra, Appl. Spectrosc. 43
485 (1989) 772–777. doi:10.1366/0003702894202201.
486 33. Z. Wang, A.C. Bovik, H.R. Sheikh, E.P. Simoncelli, Image quality assessment: from
487 error visibility to structural similarity, IEEE Trans. Image Process. 13 (2004) 600–
488 612. doi:10.1109/TIP.2003.819861.
489 34. A. Polesel, G. Ramponi, V.J. Mathews, Image enhancement via adaptive unsharp
490 masking, IEEE Trans. Image Process. 9 (2000) 505–510. doi:10.1109/83.826787.
491 35. D.A. Clausi, An analysis of co-occurrence texture statistics as a function of grey level
492 quantization, Can. J. Remote Sens. 28 (2002) 45–62. doi:10.5589/m02-004.
493 36. L.K. Soh, C. Tsatsoulis, Texture analysis of SAR sea ice imagery using gray level co-
494 occurrence matrices, IEEE Trans. Geosci. Remote Sens. 37 (1999) 780–795.
495 doi:10.1109/36.752194.
496 37. R.M. Haralick, K. Shanmugam, I. Dinstein, Textural Features for Image
497 Classification, IEEE Trans. Syst. Man. Cybern. SMC-3 (1973) 610–621.
498 doi:10.1109/TSMC.1973.4309314.
499 38. F. Marini, Classification methods in chemometrics, Curr. Anal. Chem. 6 (2010) 72–
500 79.
501 39. R. Seifi Majdar, H. Ghassemian, A probabilistic SVM approach for hyperspectral
502 image classification using spectral and texture features, Int. J. Remote Sens. 38 (2017)
503 4265–4284. doi:10.1080/01431161.2017.1317941.

504

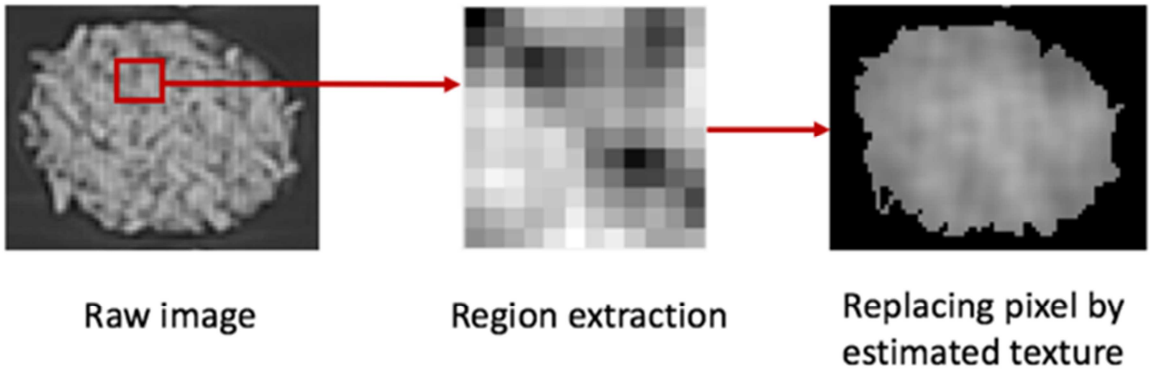


505

506 Figure 1 : Schematic of the window operation performed for extracting textural features.

507

508

509

510

511

512

513

514

515

516

517

518

519

520

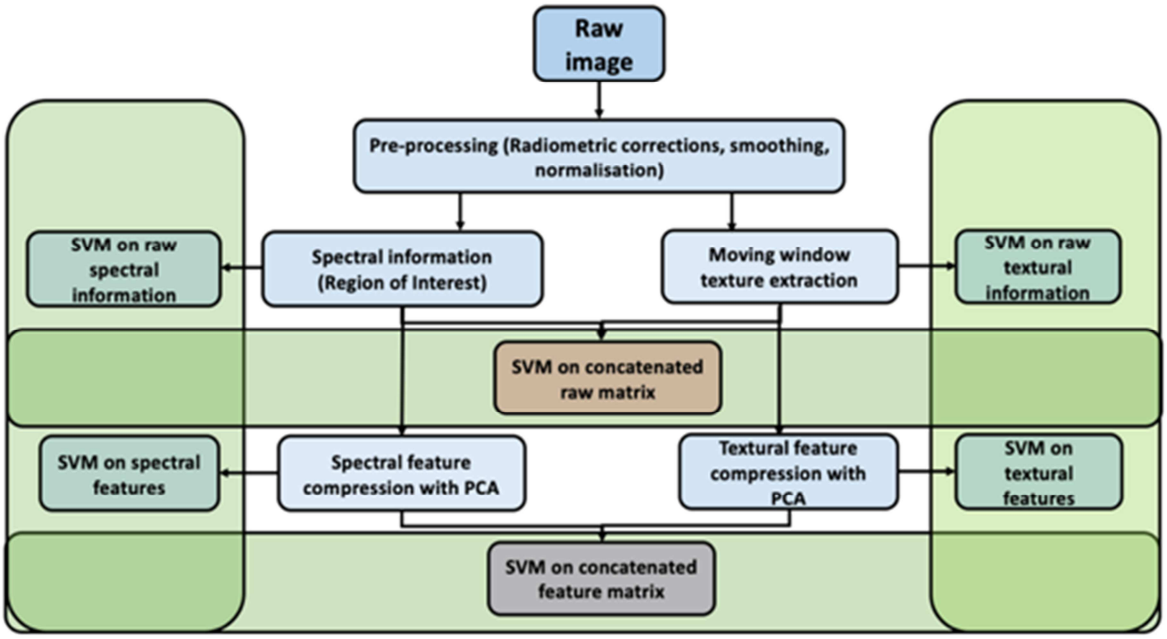


521

522 Figure 2: Schematic for raw data-level and feature-level fusion.

523

524

525

526

527

528

529

530

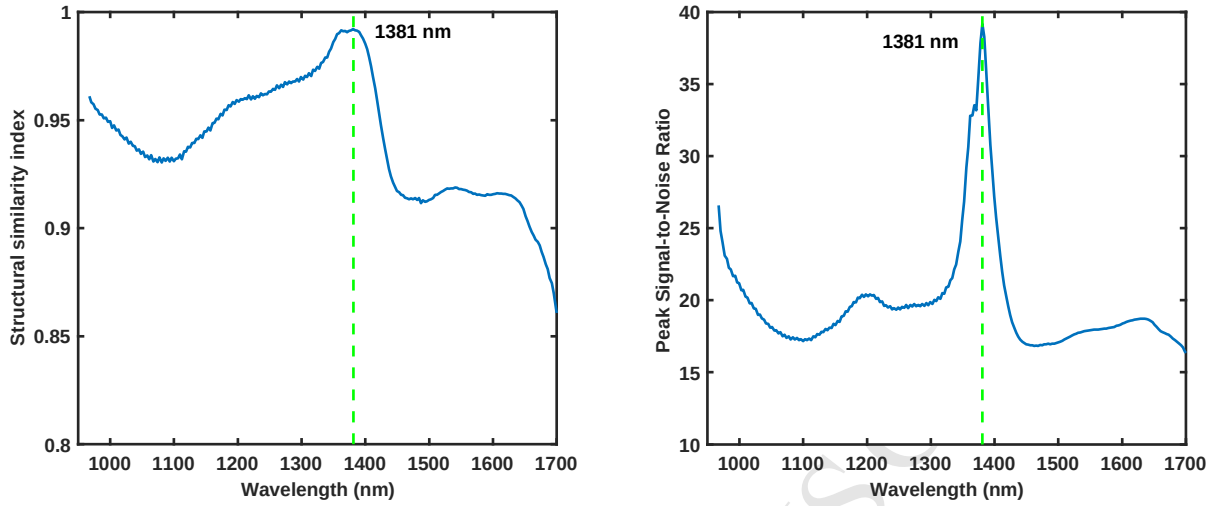


(a) (b)

Figure 3 : Criteria used for selection of the best image plane on which to perform sharpening and textural analysis: a) SSIM and b) PSNR for all image planes in the range 967.11 – 1700 nm.

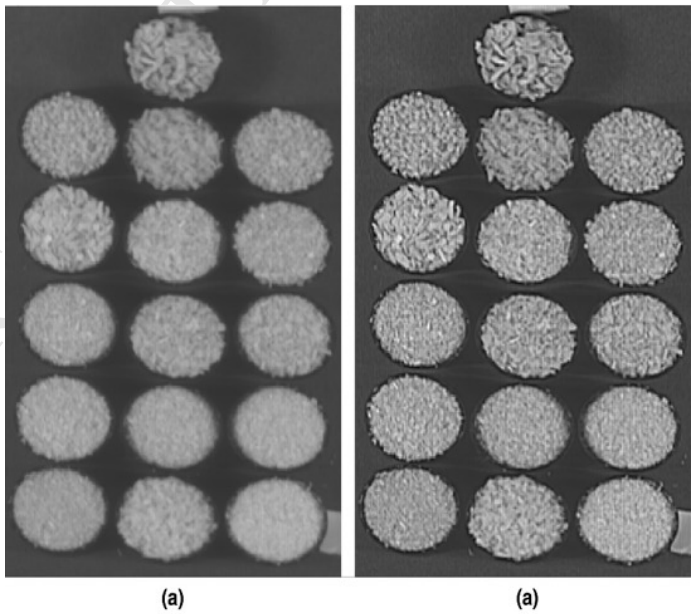


Figure 4 : Greyscale images produced using the image plane at 1381 nm (a) without and (b)

541 with sharpening.

542

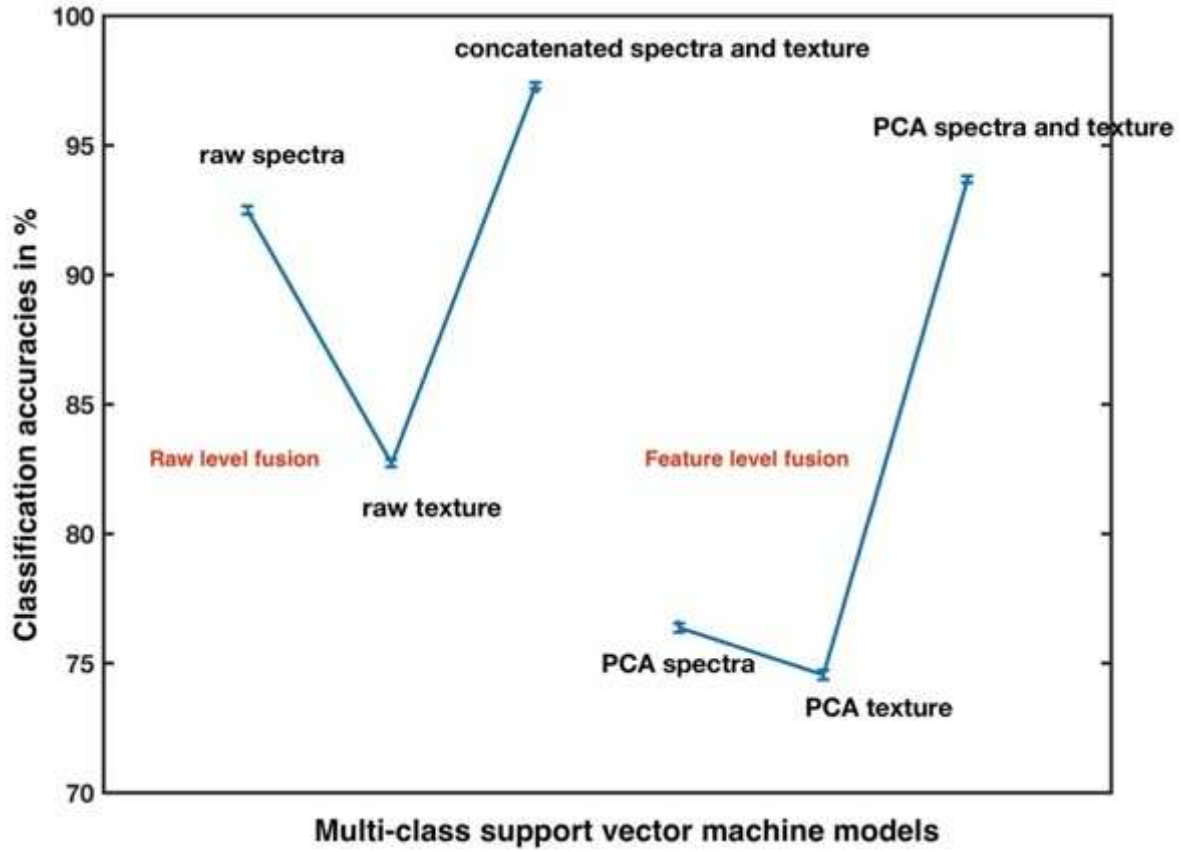


543

544 Figure 5 : Mean classification accuracies (in percent) of the 16 green tea products obtained
545 for the calibration samples (pixels) using models built with raw data and PCA features. In
546 both cases, models were built using spectral information alone, textural information alone
547 and fused spectral and textural information. The error bars denote ± 1 standard deviation (n =
548 100).

549

550

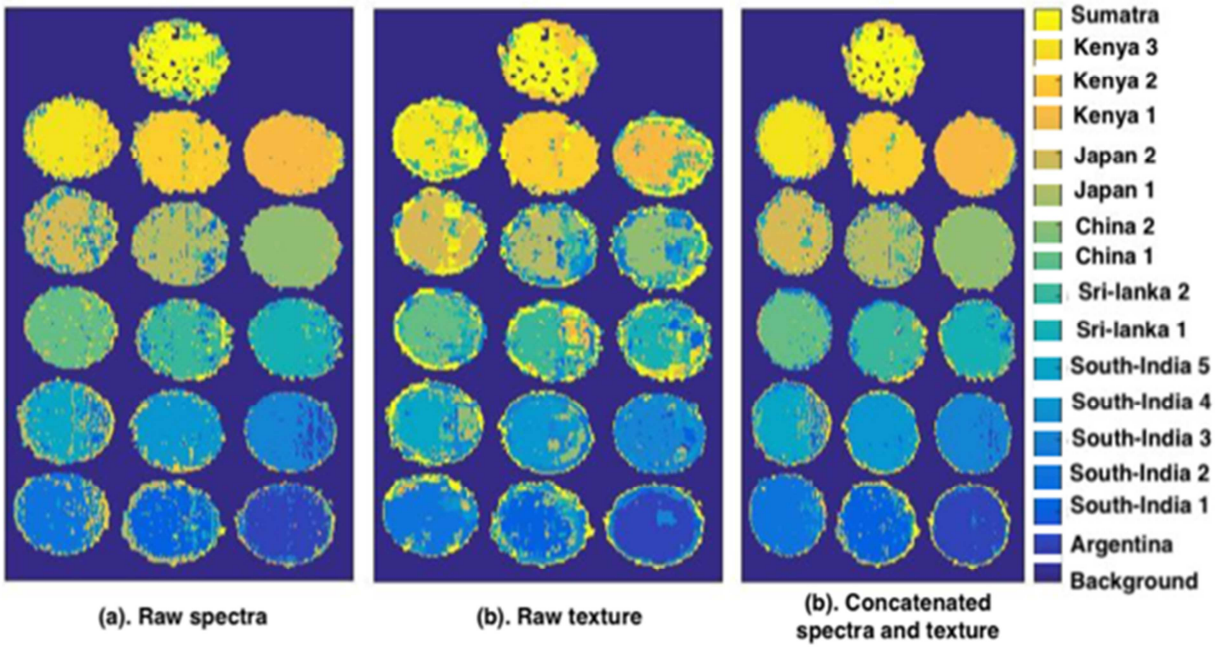


Figure 6 : Classification maps for the 16 green tea products obtained from SVM modelling of (a). raw spectral information, (b). raw textural information, and (c). concatenated raw spectral and textural information.

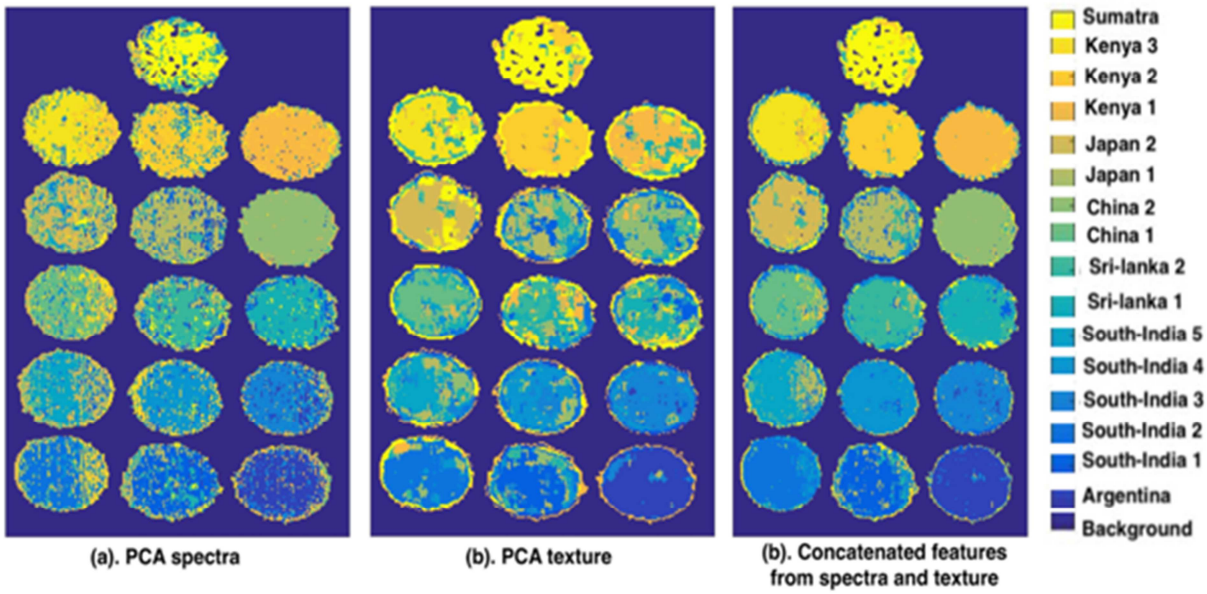


Figure 7 : Classification maps for the 16 green tea products obtained from SVM modelling of (a). PCA features extracted from spectral information, (b). PCA features extracted from textural information, and (c). concatenated PCA features from spectral and textural information.

564

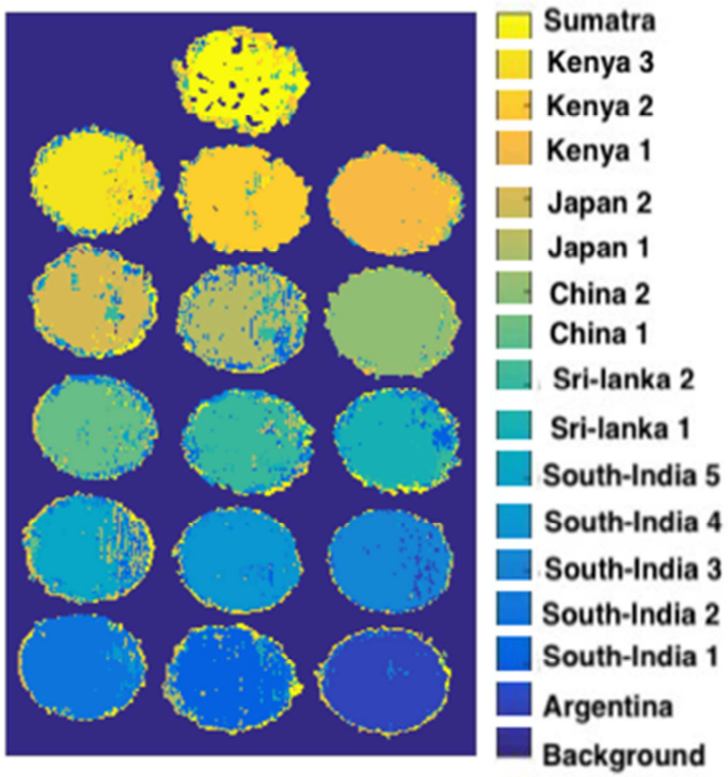


565
566

567 Figure 8 : Classification maps for the 16 green tea products obtained from decision-level data
568 fusion, using a majority voting scheme, of the six classification maps obtained from SVM
569 modelling of spectral information, textural information, and spectral and textural information
570 using raw data (Figure 6) and PCA features (Figure 7).

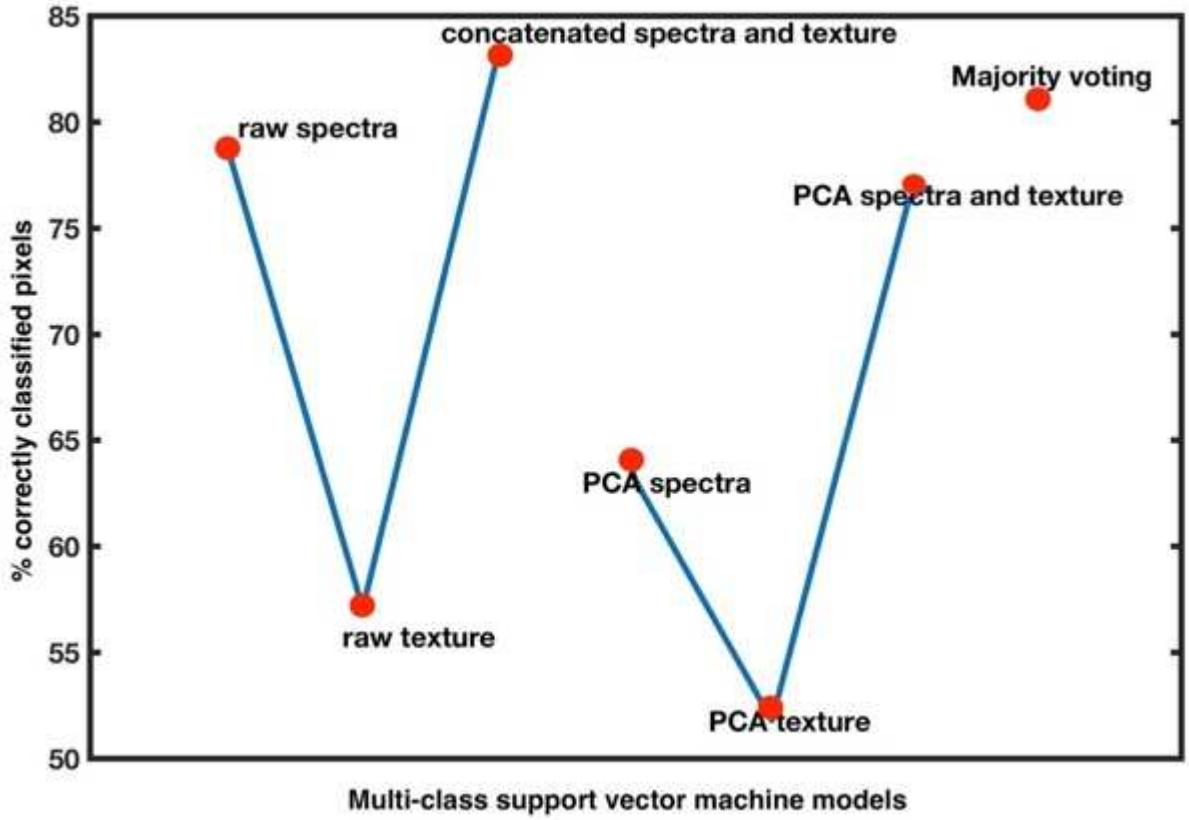


571
572
573 Figure 9 : Percentage of pixels correctly identified in the classification maps for the 16 green
574 tea products obtained using six different SVM models and decision-level fusion by majority
575 voting.
576

577

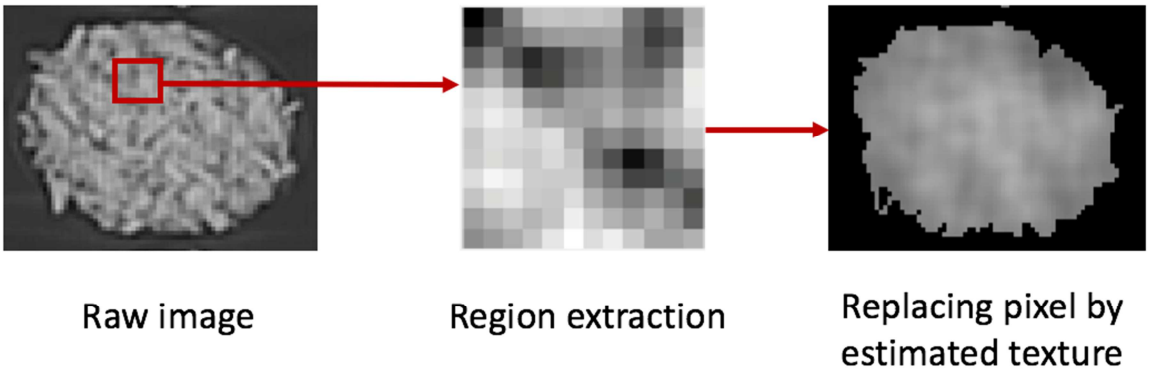


Figure 1 : Schematic of the window operation performed for extracting textural features.

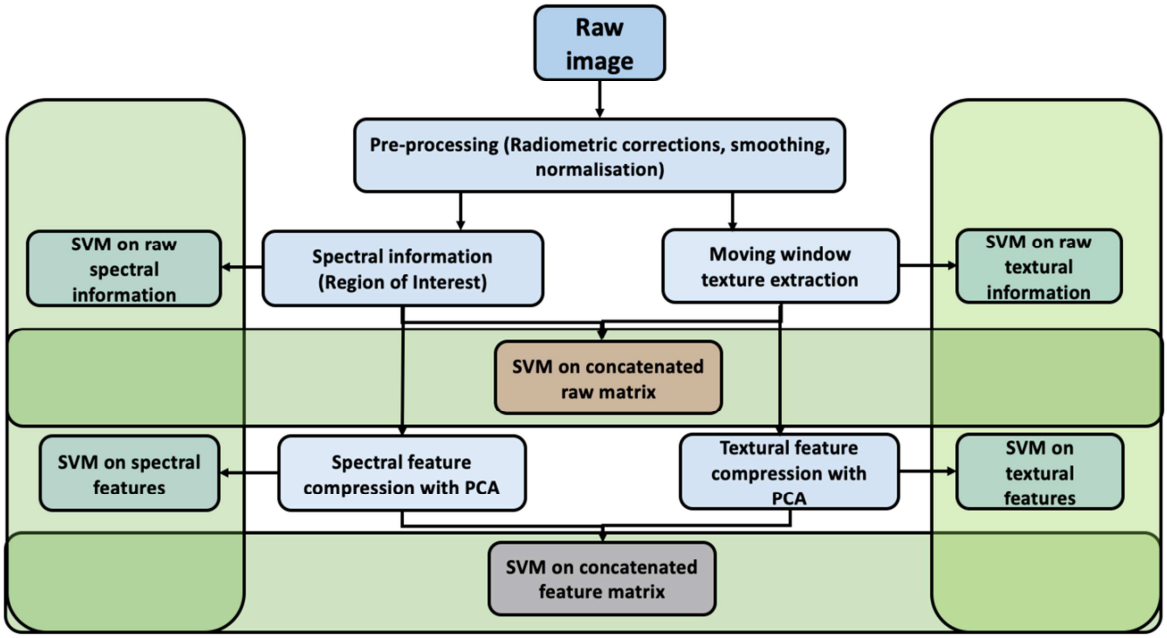


Figure 2: Schematic for raw data-level and feature-level fusion.

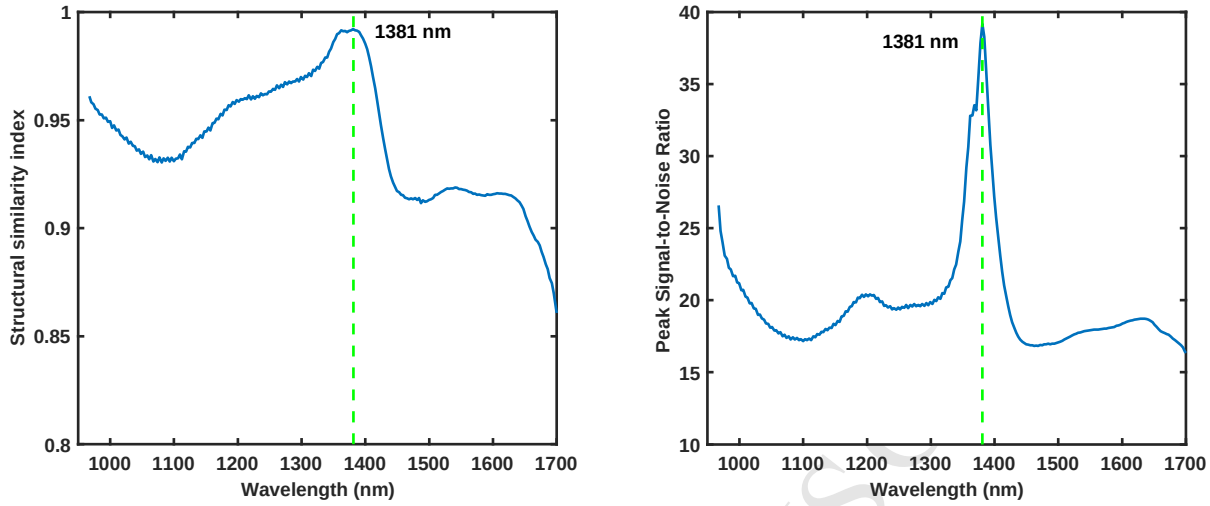


(a) (b)

Figure 3 : Criteria used for selection of the best image plane on which to perform sharpening and textural analysis: a) SSIM and b) PSNR for all image planes in the range 967.11 – 1700 nm.

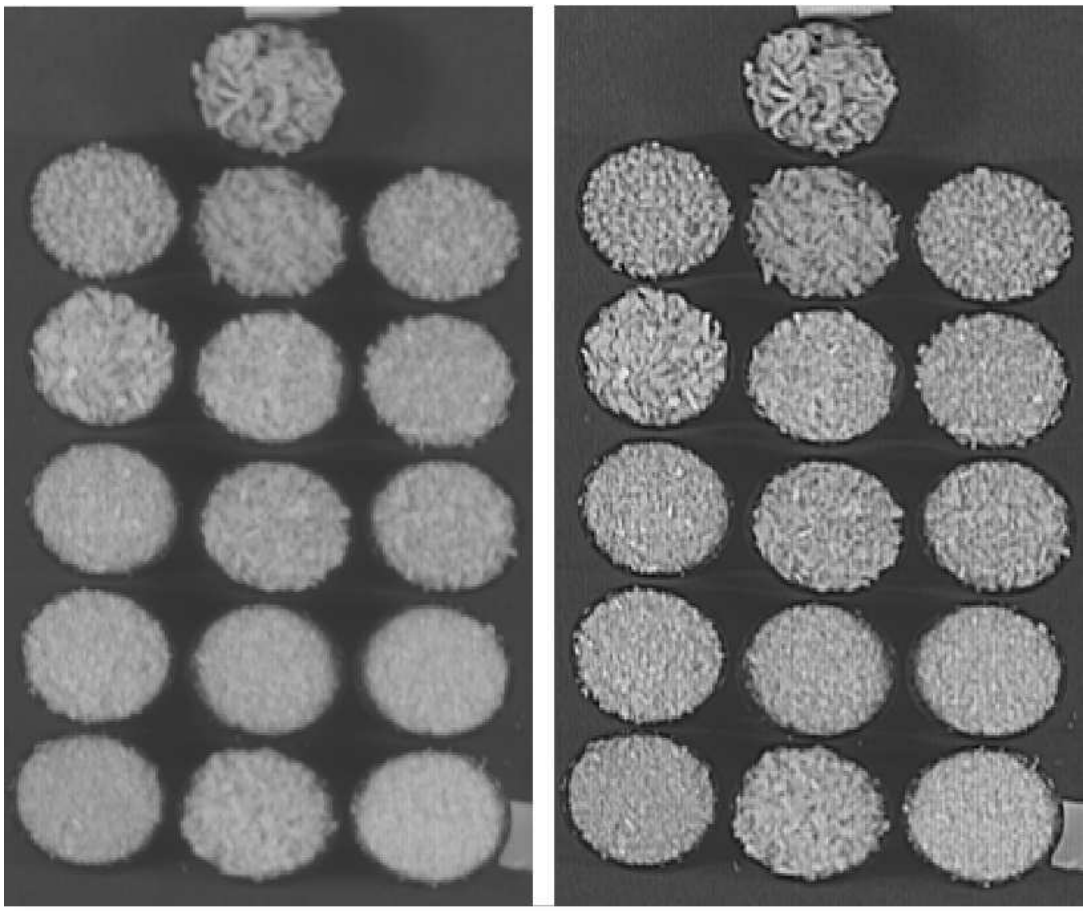


Figure 4 : Greyscale images produced using the image plane at 1381 nm (a) without and (b) with sharpening.

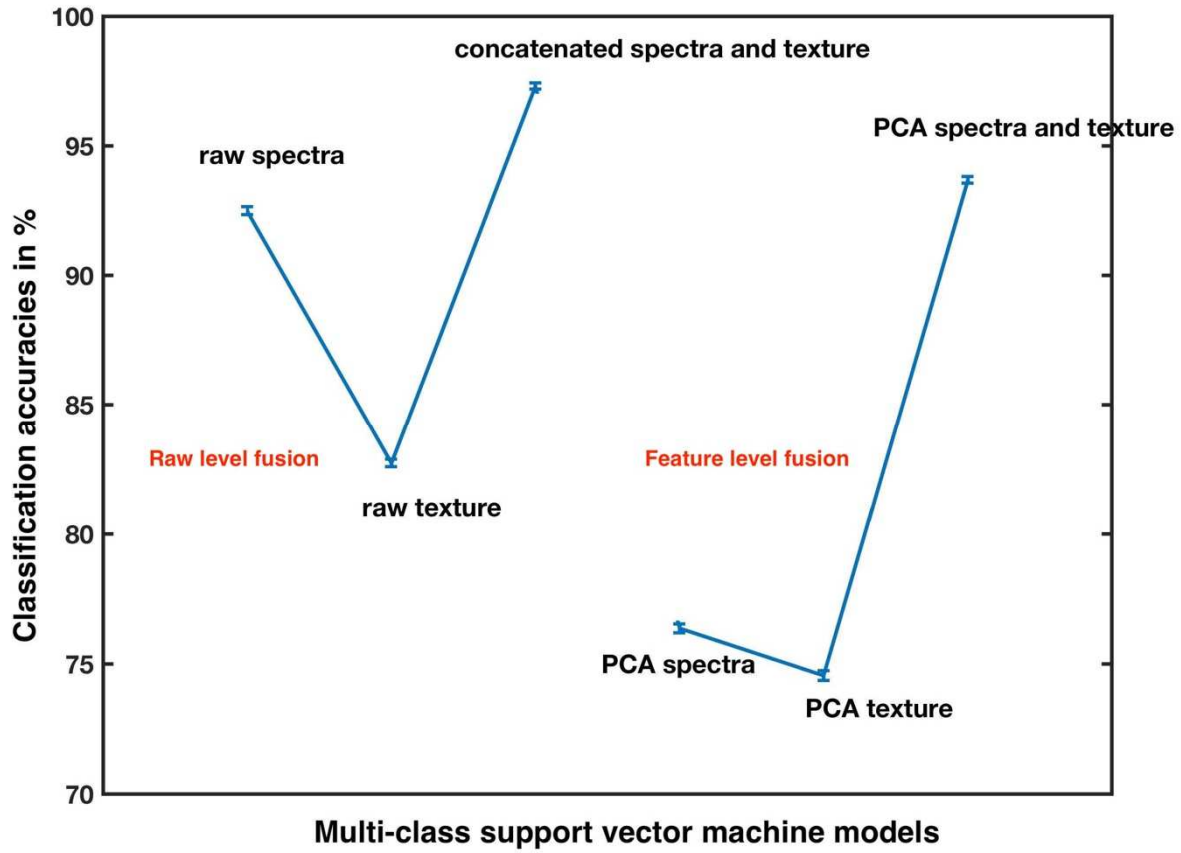


Figure 5 : Mean classification accuracies (in percent) of the 16 green tea products obtained for the calibration samples (pixels) using models built with raw data and PCA features. In both cases, models were built using spectral information alone, textural information alone and fused spectral and textural information. The error bars denote ± 1 standard deviation (n = 100).

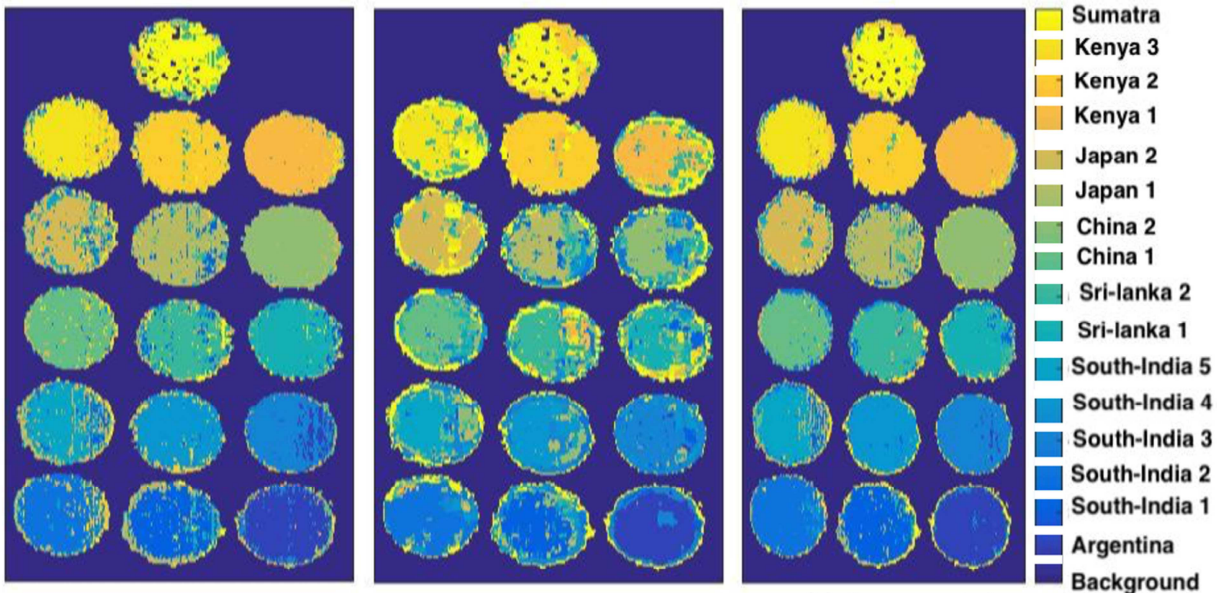


(a). Raw spectra

(b). Raw texture

(b). Concatenated spectra and texture

Figure 6 : Classification maps for the 16 green tea products obtained from SVM modelling of (a). raw spectral information, (b). raw textural information, and (c). concatenated raw spectral and textural information.

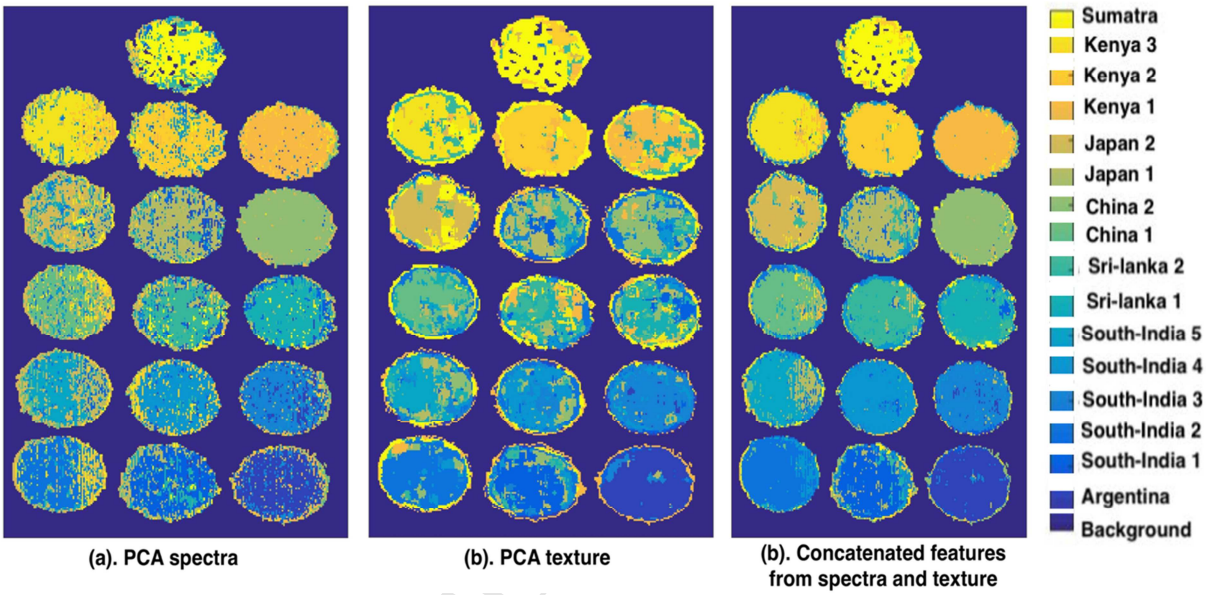


Figure 7 : Classification maps for the 16 green tea products obtained from SVM modelling of (a). PCA features extracted from spectral information, (b). PCA features extracted from textural information, and (c). concatenated PCA features from spectral and textural information.

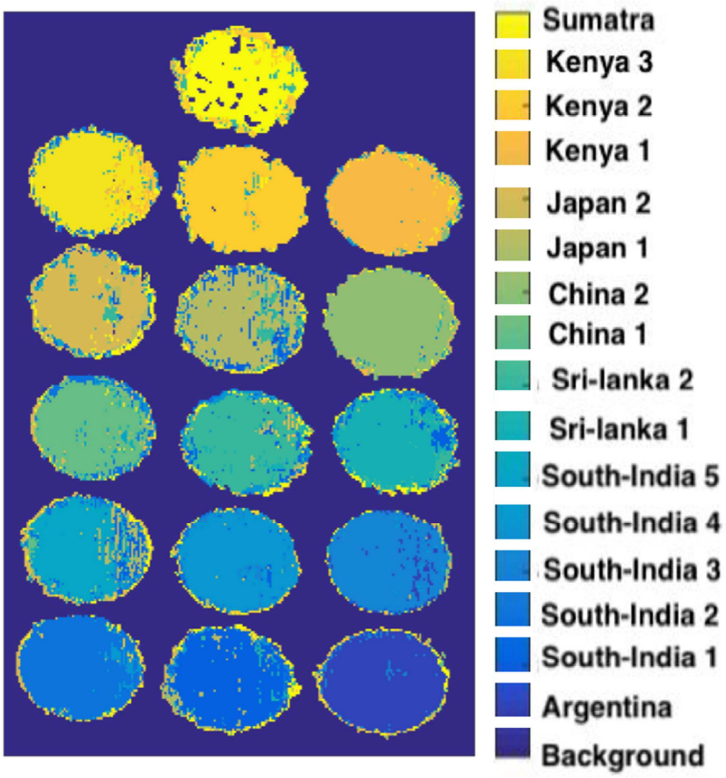


Figure 8 : Classification maps for the 16 green tea products obtained from decision-level data fusion, using a majority voting scheme, of the six classification maps obtained from SVM modelling of spectral information, textural information, and spectral and textural information using raw data (Figure 6) and PCA features (Figure 7).

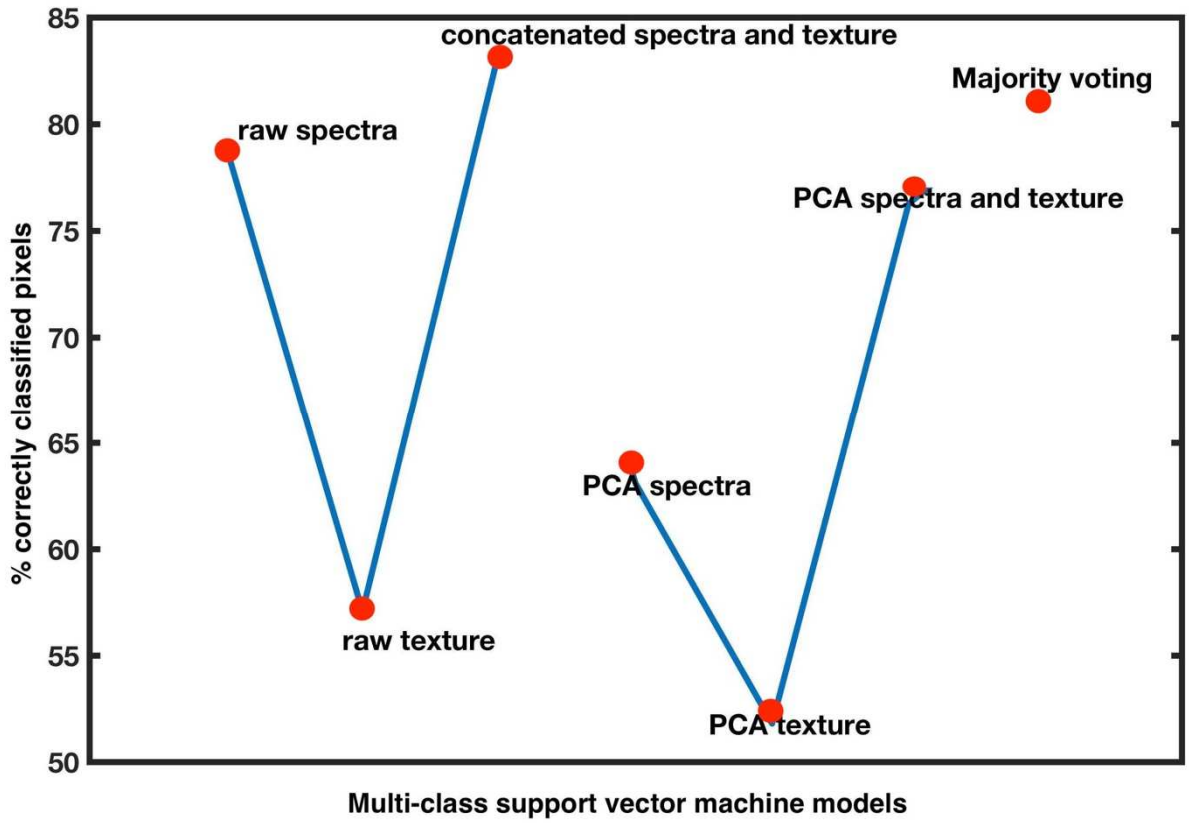


Figure 9 : Percentage of pixels correctly identified in the classification maps for the 16 green tea products obtained using six different SVM models and decision-level fusion by majority voting.

**Research highlights**

- Green tea products were analysed by near infrared hyperspectral imaging
- Textural information was extracted from the grey level co-occurrence matrix
- Textural properties were fused with near-infrared spectral information
- Data fusion improved the classification accuracy for green tea products